ISBN: 978-3-95450-234-9 ISSN: 2673-5504 doi:10.18429/JACoW-SRF2023-THIXA01

INVESTIGATION OF PLASMA PROCESSING FOR COAXIAL RESONATORS*

W. Hartung, W. Chang, K. Elliott, S. Kim, T. Konomi, K. Saito, P. Tutt, T. Xu
Facility for Rare Isotope Beams, Michigan State University, East Lansing, MI, USA

Abstract

Plasma processing has been investigated by several facilities as a method to mitigate degradation of superconducting cavity performance. It provides an alternative to removal and disassembly of cryomodules for refurbishment of each cavity via repeat etching and rinsing. Studies of plasma processing for quarter-wave and half-wave resonators were undertaken at the Facility for Rare Isotope Beams, where a total of 324 such resonators are presently in operation. Plasma cleaning tests were done on several resonators using the fundamental power coupler (FPC) to drive the plasma via the fundamental mode or a higher-order mode (HOM). HOMs allow for less mismatch at the FPC and hence lower field in the coupler relative to the cavity. Before-and-after cold tests showed a significant reduction in field emission X-rays with judicious application of plasma processing.

INTRODUCTION

Particle accelerators for electrons and ions are increasingly making use of superconducting radio-frequency (SRF) cavities to accelerate beams with high accelerating gradients at a high duty cycle. Degradation of cavity performance over time is a concern for long-term SRF accelerator operation. As traditional refurbishment of SRF cryomodules is labor-intensive, costly, and time-consuming, an alternative approach of in-situ plasma processing has been under development by several accelerator-based groups over the past few years. Results so far have been promising, with the first demonstration of plasma processing in an accelerator tunnel having been done at SNS [1]. Plasma processing development work has been done for a number of SRF cavity types, including $\beta = 1$ multi-cell cavities [2], $\beta < 1$ multi-cells [1], half-wave resonators [3, 4], and spoke cavities [5]. Plasma processing has been applied to several in-tunnel SNS cryomodules [1], an LCLS-II-style cryomodule [6], and a CEBAF cryomodule [7, 8], and has been found to help reduce both field emission (FE) and multipacting.

The Facility for Rare Isotope Beams (FRIB) is a superconducting linac for heavy and light ions. The FRIB driver linac contains 104 quarter-wave resonators (QWRs, 80.5 MHz) and 220 half-wave resonators (HWRs, 322 MHz). The linac began user operations in May 2022 [9, 10]. A pro-active campaign to develop techniques for plasma processing of FRIB cavities was undertaken starting in 2020. Preliminary results have been reported previously [11, 12]. Recent developments in this effort will be described in this paper.

* Work supported by the US Department of Energy Office of Science under Cooperative Agreement DE-SC0000661.

BACKGROUND AND APPROACH

Plasma processing is done at room temperature with a steady flow of process gases. Plasma evaluation and development can be done using a custom-length input antenna with minimal mismatch at room temperature, but in-situ processing must be done by driving the plasma via the fundamental power coupler (FPC) or via a higher-order mode (HOM) coupler. Ignition of coupler plasma is a concern, as this could produce sputtering or damage to the RF window ceramic [7, 13]. The use of HOM couplers has been found to be beneficial for $\beta = 1$ cavities [2, 7].

Features of the FRIB cavities which make plasma processing a challenge include (i) the relatively weak input coupling, which results in a lot of FPC mismatch at room temperature; (ii) the absence of HOM couplers; (iii) the relatively small access ports, which make it difficult to see the cavity's interior and gauge the location of the plasma.

Table 1 provides FRIB FPC coupling information and component counts for the FRIB linac. The FPCs have some adjustability; for plasma processing, we have set the FPC for maximum coupling strength (minimum $Q_{\mathrm{ext},1}$) to minimize the mismatch with the cavity warm. The corresponding coupling factor ($\beta_1 \equiv Q_0/Q_{\mathrm{ext},1}$) ranges from 0.2 to 2%.

The plasma processing development steps planned for the FRIB cavities are outlined in Table 2. Experimental work so far has been for the $\beta = 0.086$ QWRs and the $\beta = 0.54$ HWRs, which are the most numerous.

Plasma processing development was done with FRIB cavities leftover from production or in production as spare cavities. All of the cavities were cold-tested prior to plasma processing. At present, the cavities must be vented between plasma processing and cold tests, with a dedicated setup being used for plasma work. The assembly steps are done in a clean room environment. Either a custom-length input antenna or a spare FPC is used to drive the plasma. A shorter input antenna is used for cold tests.

Table 1: FRIB cavity counts and coupling strengths for a warm cavity. Q_0 = cavity intrinsic quality factor.

Cavity β	0.043	0.086	0.29	0.54
Quantity	12	92	72	148
Nom $Q_{\mathrm{ext},1}$	$2\cdot10^6$	$2\cdot10^6$	$6\cdot10^6$	$1\cdot10^7$
Min $Q_{\mathrm{ext},1}$	$1\cdot10^6$	$1\cdot10^6$	$3\cdot10^5$	$8\cdot10^5$
Cavity Q_0	$2\cdot10^3$	$3\cdot10^3$	$6\cdot10^3$	$9\cdot10^3$
Max β_1	$2\cdot10^{-3}$	$3\cdot10^{-3}$	$2\cdot10^{-2}$	$1\cdot10^{-2}$

ISBN: 978-3-95450-234-9 ISSN: 2673-5504 doi:10.18429/JACoW-SRF2023-THIXA01

Table 2: Plasma Processing Development Steps

Step	Started?
1 Feasibility study	yes
2 Plasma with custom input coupler	yes
3 Cavity cold test before and after	yes
4 Plasma with FPC	yes
5 Cavity cold test before and after	yes
6 Repeat 4 & 5 without venting in between	no
7 Repeat 4 & 5 for offline cryomodule	no

PLASMA PROCESSING DEVELOPMENT

Mismatch Mitigation with HOMs

If plasma is ignited in the FPC, we risk to damage it. Driving the plasma with an HOM via the FPC was explored as a means to reduce the FPC mismatch and reduce the risk of coupler ignition. Such an approach was found to be promising for PIP-II spoke cavities [5].

Network analyzer measurements were done to evaluate the coupler mismatch for different modes of the $\beta = 0.54$ HWR (Fig. 1) and the $\beta = 0.086$ QWR [12]. In both cases, there is less FPC mismatch as the frequency increases, such that we eventually can achieve close to unity coupling (green line). Custom antennae with near-unity coupling for the fundamental model are generally overcoupled for HOMs.

For the $\beta = 0.086$ QWR, plasma measurements were done for the first 3 modes [12, 14], and processing was done with the first and third modes (TEM $\lambda/4$ and $5\lambda/4$). Work on the $\beta = 0.54$ HWR is presently focused on modes at 322 MHz, 800 MHz, and 1.35 GHz, as the latter 2 may have axial symmetry similar to the fundamental mode. Other modes may be useful for plasma processing as well.

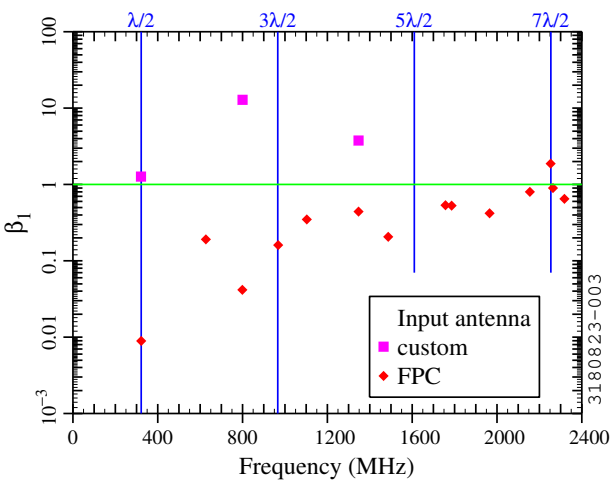

Figure 1: Network analyzer measurements of input coupling factors for some of the modes in a FRIB $\beta = 0.54$ HWR at room temperature. Red diamonds: FPC; magenta squares: custom input antenna. Blue lines: odd harmonics of the fundamental. Green line: unity coupling.

Plasma Generation and Monitoring

A steady flow of inert gas is used for plasma processing [11, 12]. Most tests were done with neon plus a few percent of oxygen, with a cavity pressure of about 100 mTorr.

Plasma reduces the effective permittivity, which shifts the resonant frequency of the cavity; the plasma density can be inferred from the frequency shift [15, 16]. In recent plasma measurements, we used a network analyzer to monitor the resonant frequency while driving the plasma with an independent generator. With this method, the drive frequency can be raised to match the resonant frequency after it is shifted by the plasma, but this must be done iteratively because the plasma density increases as the drive frequency increases. Our approach was based on similar work for LCLS-II [17] and CEBAF [7] cavities. A modified RF circuit was used, as shown in Fig. 2, due to the narrower circulator bandwidths at lower frequencies.

Viewports allow for optical spectroscopy measurements to make inferences about the plasma properties [11] or for imaging of the plasma with digital cameras [12].

For most plasma measurements, a bias T (without applied DC bias) was used to monitor the DC current from the input coupler using a picoammeter or multi-meter. The QWR pickup probe currents were monitored as well, but the HWR pickup loops were not.

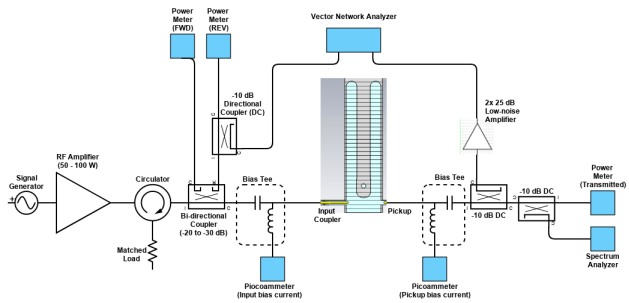

Figure 2: Schematic of the RF system used for plasma measurements and processing. Attenuators (not shown) are used to adjust the signal level as needed. The low-noise amplifier is used for just the signal to the network analyzer or is moved further upstream to amplify the other P_t signal channels.

PLASMA OBSERVATIONS

Fixed Drive Frequency

Figure 3 shows some examples of plasma generation with a constant drive frequency. The plasma is ignited in a $\beta = 0.086$ QWR using the $5\lambda/4$ HOM (~ 400 MHz). The forward power (P_f) is ramped up at a rate of 0.1 dB per second. The forward, reverse (P_r), and transmitted (P_t) power are measured during the ramp-up (P_t = power from the pickup antenna). A spectrum analyzer is used to measure P_t due to the small signal level after ignition. The stored energy U can be inferred from P_t, assuming a constant pickup coupling strength $Q_{\text{ext},2}$ (though this might not be exactly correct when plasma is present).

ISBN: 978-3-95450-234-9 ISSN: 2673-5504 doi:10.18429/JACoW-SRF2023-THIXA01

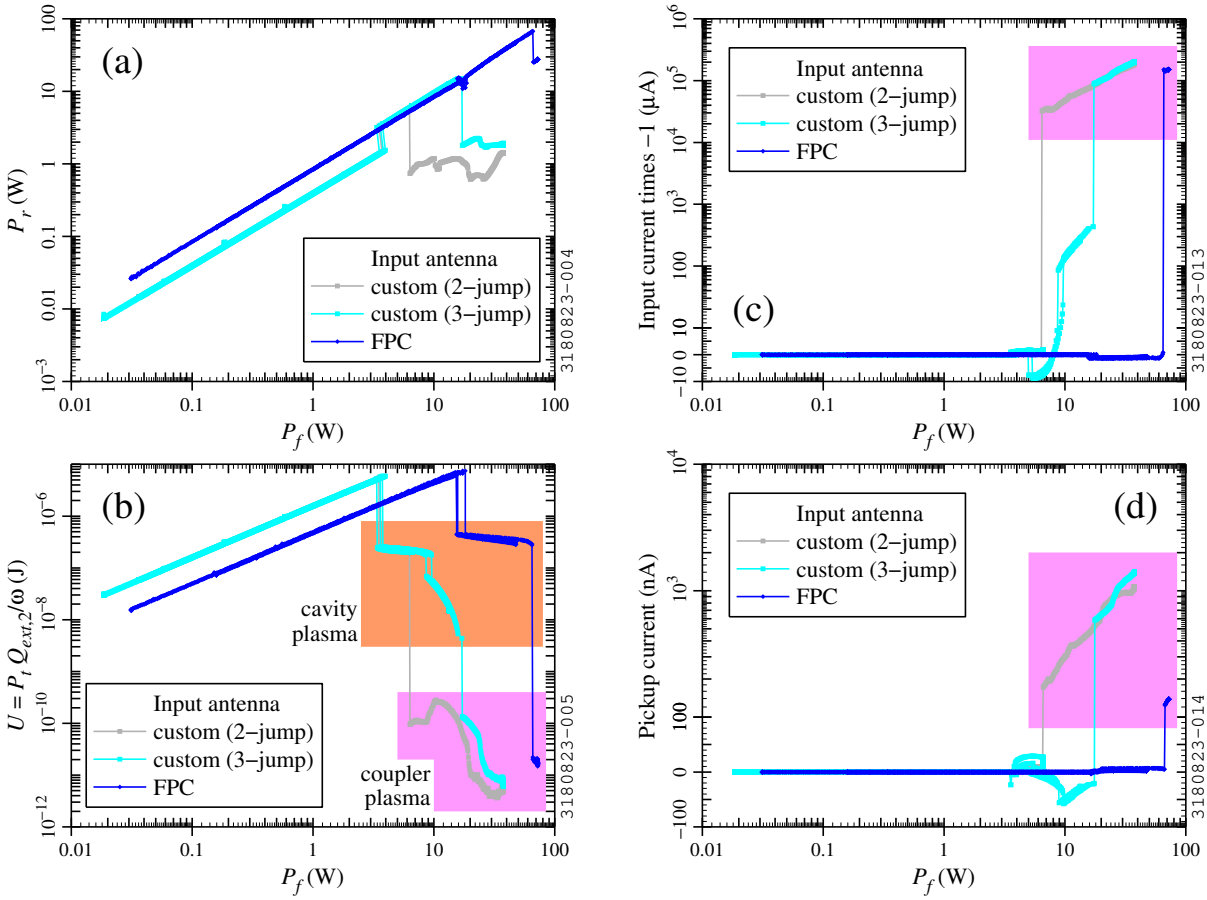

Figure 3: Measurements on $\beta = 0.085$ QWRs, driving the plasma via the TEM $5\lambda/4$ mode with constant drive frequency. Cyan and gray: with custom input antenna (S85-986). Dark blue: with FPC (S85-987).

At low P_f, the gas is neutral: P_r and P_t increase linearly with P_f and the DC currents are approximately zero, as one would expect. Then plasma is ignited in the cavity, producing a downward jump in P_t into the orange zone of Fig. 3b. With a custom antenna, an upward jump in P_r is seen, but there is very little change in P_r for the FPC (as $P_r \approx P_f$ already at low power). The jumps are the result of a drop in the cavity quality factor (Q_0) due to the additional power loss into ionization of the gas and the shift in the resonant frequency due to the plasma. Small DC currents are seen on both antennae. Dim light from the plasma is seen after cavity plasma ignition.

As P_f increases further, a second downward jump in P_t is seen in some cases (cyan), without a jump in P_r, but with a jump in the DC currents. Evidently this is due to cavity plasma ignition moving or expanding to a different location. In other cases (gray, blue), there is no such jump. The second jump is seen with a custom antenna for all 3 QWR modes, but not in the HWR or with the FPC.

As P_f increases further, another downward jump in P_t is seen into the pink zone of Fig. 3b, along with a downward jump in P_r; the current from both antennae increases sharply. The decrease in both P_t and P_r indicates that the power is mainly being absorbed by the plasma as the RF wave travels through the coupler, rather than going to the cavity. With coupler plasma ignited, bright reflected light is produced, the input coupler current is about −100 mA, and the pickup current reaches up to about 1 μA.

Several measurements are shown in Fig. 3 for both the custom antenna and FPC cases. Cavity ignition occurs at approximately the same U for both the custom antenna and the FPC (Fig. 3b). However, there is some scatter in thresholds and variability in DC currents from one measurement to another. More importantly, coupler ignition sometimes happens at a significantly lower P_f with a custom input antenna, as seen in the contrast between the gray and cyan curves. The intermediate jump for the cyan cases likely corresponds to production of a more dense or more widespread cavity plasma; this is not seen with the FPC (dark blue).

When ramping the drive power back down, the plasma can be sustained at power levels below the ignition threshold. In some cases, the coupler plasma persists until extinction without a return to cavity plasma.

Varying the Drive Frequency

As described above, the plasma shifts the cavity resonant frequency up. Figure 4 shows an example: network analyzer (NA) measurements of S_{21} for different drive frequencies.

ISBN: 978-3-95450-234-9 ISSN: 2673-5504 doi:10.18429/JACoW-SRF2023-THIXA01

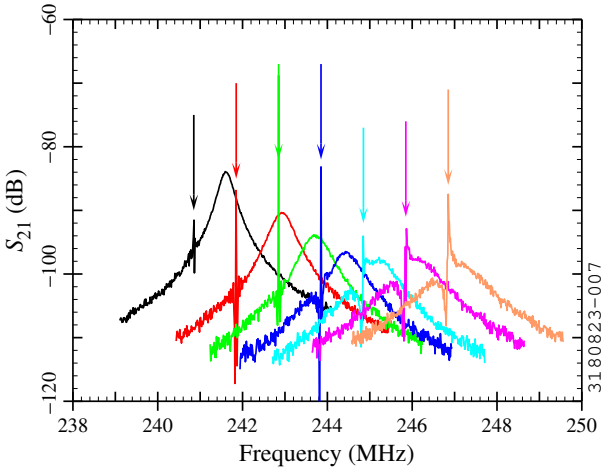

Figure 4: NA measurements on the TEM $3\lambda/4$ mode of a $\beta = 0.085$ QWR with a custom antenna: transmission coefficient as a function of frequency with constant P_f for different drive frequencies (arrows).

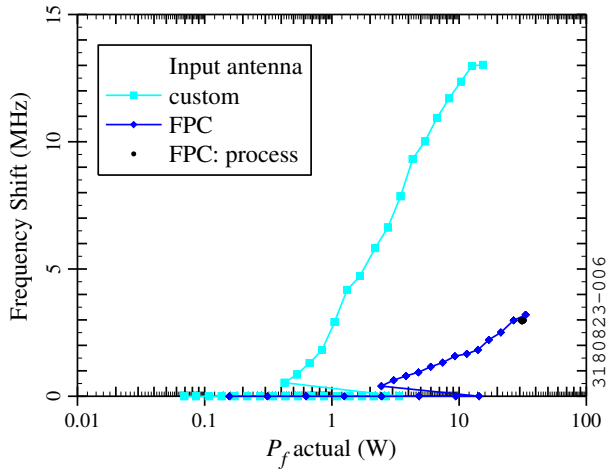

Figure 5: Measurements on $\beta = 0.085$ QWRs: resonant frequency of the TEM $5\lambda/4$ mode as a function of drive power with a custom input antenna (cyan, S85-986) and with the FPC (blue, S85-987). The drive frequency is increased to be near the maximum. Black circles: power and frequency shift for plasma processing with the FPC.

At low power, the resonant frequency is 240.85 MHz (black arrow); after ignition, the resonant frequency shifts up (black curve). The NA shows the cavity resonance curve plus a narrow-band signal at the drive frequency. When the drive frequency is increased by 1 MHz (red arrow), the resonant frequency shifts up by more than 1 MHz (red curve). With step-wise increases in the drive frequency, eventually the drive frequency approaches the resonant frequency (orange). As the plasma density increases, more power is delivered to the plasma, Q_0 decreases, and the bandwidth increases. If we continue to increase the drive frequency, either we return to neutral gas or we ignite the coupler. By raising the drive frequency to be close to the limit, we can produce a more dense plasma and drive the cavity closer to resonance: in Fig. 4, with constant drive frequency, the resonant frequency shift is <1 MHz; with iterative increase of the drive frequency, the resonant frequency shift is >6 MHz.

An example of plasma generation with drive frequency adjustment is shown in Fig. 5. The resonant frequency is monitored with the NA and the drive frequency is raised to be near the limit. At low power, there is no frequency shift. When the cavity plasma turns on, we observe a frequency shift which increases with P_f. In this example, the maximum frequency shift is $\sim$ 13 MHz with a custom input antenna (cyan), limited by coupler ignition. Unsurprisingly, the maximum frequency shift is smaller ($\sim$ 3 MHz) for the FPC case (dark blue) and higher P_f is needed. The corresponding plasma densities are estimated to be $1.3 \cdot 10^{14}$ m^{-3} with the custom antenna and $3.2 \cdot 10^{13}$ m^{-3} with the FPC.

RF Power for Plasma Ignition

Figure 6 summarizes measurements of the forward power for cavity plasma ignition (light and dark green) and coupler ignition (red and magenta) with a custom input antenna (light colors) or an FPC (dark colors). Higher P_f is needed for ignition with the FPC. The ignition power increases with frequency. The P_f range for stable cavity plasma tends to be narrower with the FPC; this is particularly evident for the 80.5 MHz mode of the QWR.

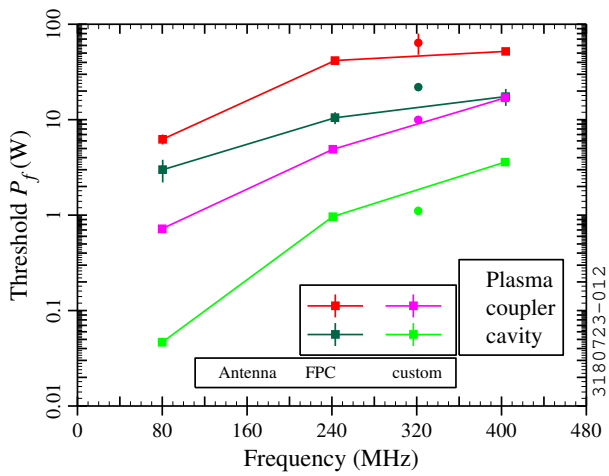

Figure 6: Measured plasma ignition thresholds for the $\beta = 0.086$ QWR (squares) and $\beta = 0.54$ HWR (circles).

The coupler ignition threshold tends to be a bit higher with constant drive frequency and a bit lower when we adjust the drive frequency to maximize the frequency shift. This suggests that a higher plasma density in the cavity helps to facilitate ignition in the coupler. Furthermore, we have observed early coupler ignition in some cases (as seen in Fig. 3). With the TEM $3\lambda/4$ mode of the QWR, we sometimes are able to reach the maximum power without coupler ignition (as discussed further in the next section). Hence the error bars in Fig. 6 may be underestimated.

ISBN: 978-3-95450-234-9 ISSN: 2673-5504 doi:10.18429/JACoW-SRF2023-THIXA01

Frequency Shift Due to Cavity Plasma

Figure 7 shows the frequency shifts we have been able to reach with a custom antenna (cyan) or an FPC (blue). The square markers show the first 3 modes of the QWR; the hollow squares for the 240 MHz case reflect the observation that sometimes we are able to reach higher density with low light production and low current, limited by available RF power. For other cases, the limit is coupler ignition.

The frequency shift is less for the FPC cases than for the custom input antenna, again, unsurprisingly. In both cases, we generally observe a higher frequency shift and a higher plasma density for higher frequencies.

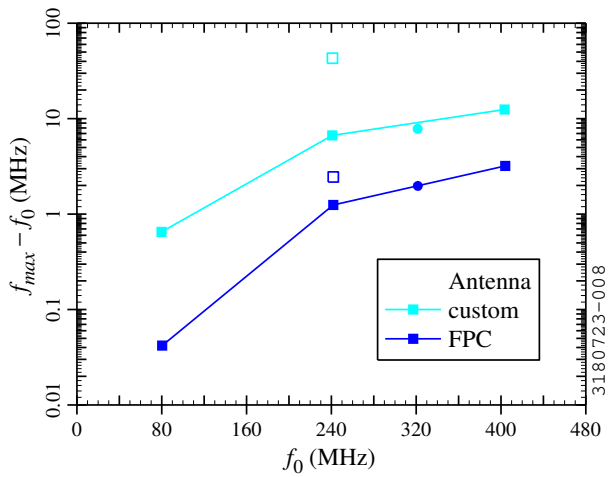

Figure 7: Maximum measured frequency shift due to the plasma for the $\beta = 0.086$ QWR (squares) and $\beta = 0.54$ HWR (circles).

PLASMA PROCESSING

Methods

The plasma ignition field increases approximately linearly with frequency. At low frequency, cavity plasma ignition happens at low field with dim light and little generation of reaction by-products. As a result, some time and effort were needed for us to distinguish between cavity plasma and coupler plasma. For the first several plasma processing trials, we tried to achieve a bright plasma, which, according to our present understanding, had the undesired consequence that we produced coupler plasma rather than cavity plasma.

In recent trials, we tried to avoid coupler plasma. For our updated method, we drive the cavity plasma just below the drive power and drive frequency limits to process with a near-maximum plasma density, anticipating that this corresponds to a near-maximum cleaning efficiency. We were able to produce a stable cavity plasma for processing, with no accidental coupler ignition.

The TEM $5\lambda/4$ mode was selected for processing of the QWR with the FPC, as, of the lowest 3 modes, it allows for the highest frequency shift and the least FPC mismatch. The measured drive power and frequency shift during plasma processing are included in Fig. 5 (black circles) above.

So far, plasma processing for the HWR has been done only using the fundamental mode, with the 800 MHz and 1.35 GHz HOMs not having been found very suitable for the custom input antenna case; investigation of HOMs for the FPC case is still in progress.

Reaction By-Products

A residual gas analyzer (RGA) is used to monitor the reaction by-products during plasma processing. The RGA samples some of the gas pumped through the system; a leak valve is used to maintain lower pressure at the RGA to avoid overloading it. When the plasma is ignited, the RGA shows an increase in CO_2, CO, and H_2O, and a decrease in O_2. These signals are short-lived, as described in Ref. [12].

The RGA peaks return if the plasma is re-ignited the next day, consistent with observations at SNS [18]. The RGA signals trend downward with repeated iterations, as seen in Fig. 8, which shows the change in partial pressure after plasma ignition (ΔP_m) for selected mass numbers (m), normalized to the partial pressure of neon (P_{20}). Use of the normalized pressure change helps to compensate for slow variations in the residual gas composition and RGA sensitivity over time, as well as inexact resetting of the leak valve position between trials. As seen in Fig. 8, the by-product pressures are initially as large as ~ 10% of the Ne pressure; they decrease with repeated processing iterations, but increase if the daily processing cycle is paused for the the weekend. In the coupler plasma case (left), the signals were small but non-zero after 13 iterations. In the cavity plasma case (right, with a time offset added for clarity), the signals were already relatively small (though non-zero) when plasma processing was discontinued after 5 iterations.

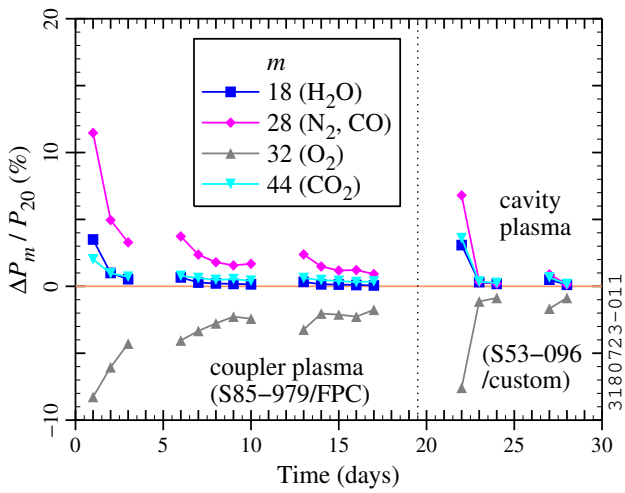

Figure 8: Long-term trends for selected masses from RGA measurements. Left: coupler plasma for a $\beta = 0.086$ QWR with FPC. Right: cavity plasma for a $\beta = 0.54$ HWR with custom antenna.

ISBN: 978-3-95450-234-9 ISSN: 2673-5504 doi:10.18429/JACoW-SRF2023-THIXA01

COLD TEST RESULTS

For the $\beta = 0.086$ QWR case, cold test results for the first plasma processing trials with a custom antenna and with an FPC were presented previously [11, 12]. However, we now understand that these trials were all done with coupler plasma rather than cavity plasma.

QWR with FPC: Cavity Plasma

One QWR (S85-987) was plasma-processed with the TEM $5\lambda/4$ mode and FPC using the new method described above. As seen in Fig. 9a, before-and-after measurements at 2 K showed a significant reduction in FE X-rays after plasma processing. After plasma processing, no X-rays were observed up to the highest field that we were able to reach with the available RF power. There was little change in Q_0 due to plasma processing.

HWR with Custom Antenna: Cavity Plasma

One HWR (S53-096) was plasma-processed using the new method, driving the plasma with the fundamental mode using a custom antenna. As shown in Fig. 9b, no FE X-rays were observed after plasma processing. The cavity field was limited by early thermal breakdown. The field limit was a bit higher before plasma processing, but the difference is likely within the systematic errors in the measurements. Again, there was little change in Q_0 with plasma processing. The lack of X-rays after plasma processing is encouraging, but, as we were not able to reach a very high field, this result does not yet provide a very definitive conclusion about the impact of plasma processing for FRIB HWRs.

Cumulative Results

Table 3 summarizes the plasma processing trials done so far on FRIB cavities. A total of 11 rounds of plasma tests have been completed, using a total of 7 cavities, with a total of 10 before-and-after tests. In a majority of cases (green highlights in Column 6), a reduction in FE X-rays was observed after plasma processing.

However, as seen in Column 7, only 1 of the tests was done with no plasma ignition in the coupler. For cases labeled "cavity & coupler," the coupler was ignited in the plasma measurements phase, but cavity plasma was used in the processing phase. The $\beta = 0.54$ HWR appears vulnerable to sputtering of copper when the coupler plasma is ignited even for a short time. This is in contrast to the $\beta = 0.086$ QWR case in which we did not observe damage to the coupler even after more than 10 hours of cumulative coupler plasma processing, and coupler plasma processing improved the cavity performance in most cases.

Though the results for the QWRs are encouraging, more experience with plasma processing with the FPC would be desirable for both the QWRs and the HWRs.

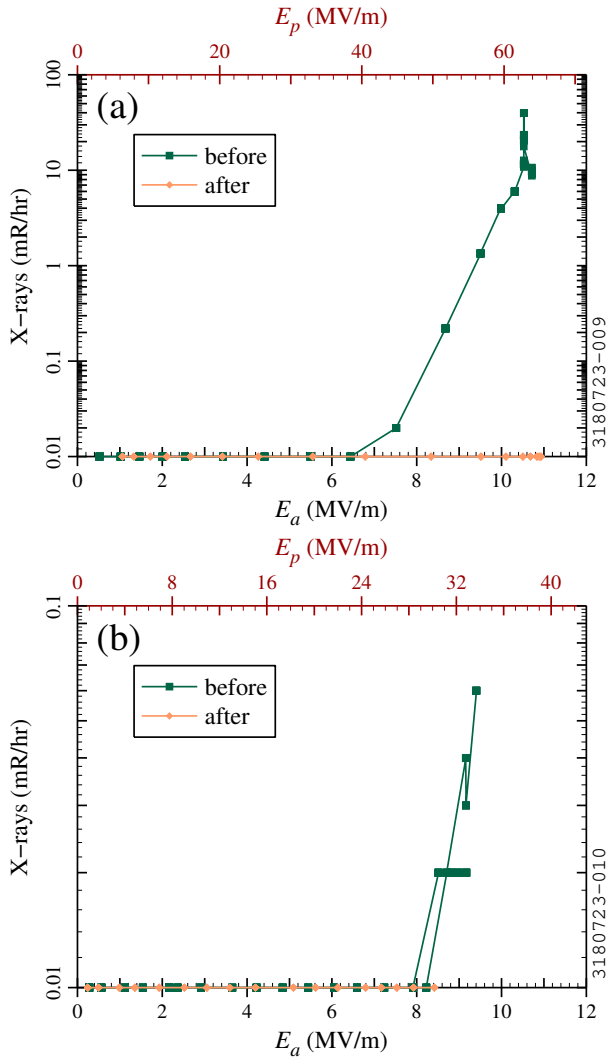

Figure 9: Measured X-rays at ~ 2 K as a function of accelerating gradient (E_a) before and after plasma processing of (a) $\beta = 0.086$ QWR with FPC; (b) $\beta = 0.54$ HWR with custom antenna. E_p: peak surface electric field.

CONCERNS

Sputtering

We have observed sputtering from the (custom) copper input antenna onto the niobium beam port for 2 HWR plasma development tests (an example is shown in Fig. 10). So far, we have not observed any sputtering in the QWRs. We have not observed sputtering in cases in which plasma was ignited only in the cavity and the pressure was kept near 100 mTorr; however, we need more experience to ensure that we avoid sputtering in the future.

We observed discoloration of the copper antenna for the custom input coupler in 2 cases. The first case appeared to be oxidation. In the second case, graying of the antenna was seen, but we did not ascertain whether this was due to oxidation or sputtering of niobium.

ISBN: 978-3-95450-234-9 ISSN: 2673-5504 doi:10.18429/JACoW-SRF2023-THIXA01

Table 3: Plasma processing tests on FRIB cavities. FE: field emission; CS: copper sputtering observed in RF port.

Date	S/N	Input coupler	Harmonic number	FE onset (MV/m)		Plasma Location	Notes
				before	after		
β = 0.086 QWRs							
May 2021	986	custom	1	5	8	coupler	[11]
May-Jun 2021	986	custom	1	8	6	coupler	[11]
Jul 2021	986	custom	1	6	8	coupler	
Oct 2021-Jan 2022	967	FPC-in	1, 3, 5	6.4	10	coupler	[12]
Feb-Mar 2022	979	FPC-in	5	7	> 10	coupler	[12]
May-Jun 2022	972	FPC-in	5	6.6	7	coupler	[12]
Jul 2022-Jan 2023	986	custom	1, 3, 5	6	9	coupler	
May-Jun 2023	987	FPC-in	1, 3, 5	7	≥ 11	cavity & coupler	Fig. 9a
β = 0.54 QWRs							
May 2020-Mar 2021	150	custom	1			coupler	CS [11]
Feb-Mar 2023	155	custom	1, 3	4.7	3	cavity & coupler	CS; Fig. 10
Apr 2023	096	custom	1	8.2	≥ 8.4	cavity	Fig. 9b
Jun 2023-	096	FPC-in	1, 3, 5			cavity & coupler	in progress

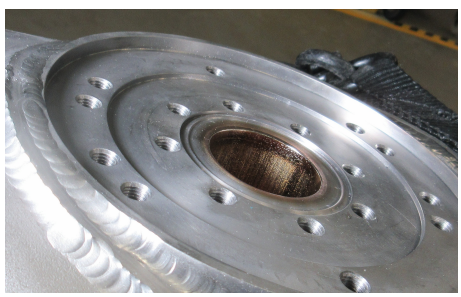

Figure 10: Photograph of the RF port of a β = 0.54 HWR after coupler plasma ignition with a copper antenna.

Plasma Uniformity and Repeatability

As seen above, the cavity plasma sometimes jumps to a higher-density state and sometimes jumps directly to coupler plasma (Fig. 3b); in some cases, the plasma brightness is reduced and coupler ignition does not occur, but a higher frequency shift can be reached (Fig. 7, solid vs hollow squares). Though we expect the plasma distribution to be determined by the electric field distribution, these observations suggest that the plasma might not always ignite throughout the high-field regions. This may be analogous to the multi-cell cavity case: when a multi-cell cavity is driven in the π mode, such that all of the cells have approximately the same field, ignition happens randomly in only 1 of the cells [19]. This indicates that there may be room for improvement in our methods, as a uniform plasma distribution and repeatable plasma ignition are likely to produce better outcomes.

CONCLUSION

Our results so far suggest that plasma processing has good potential for improving FRIB resonators. Higher-order modes look promising as a way to drive the plasma. However, processing of a FRIB HWR with an FPC has not yet been attempted. Damage to the FPC and uniformity of the plasma distribution are still items of concern. Alternative plasma processing approaches have been explored by other groups, and these may be beneficial for FRIB cavities.

Additional steps on FRIB cavities include testing plasma processing with a cryomodule and attempting plasma processing in the FRIB tunnel. Parallel efforts include 3D RF model development to better understand the cavity and coupler fields; and using the models and plasma theory to predict ignition thresholds for the cavity and coupler [14].

With our present approach, it is difficult to assess how long the cavity should be processed for optimum results. The effectiveness of plasma processing may depend on the nature of the contaminants.

ACKNOWLEDGMENTS

Early work at FRIB on plasma development, measurements, and analysis was led by Cong Zhang. John Popielarski provided valuable guidance and support for the FRIB plasma efforts until his untimely passing in 2022. Jacob Brown and Sara Zeidan assisted with recent plasma measurements. We thank Pete Donald, Dave Norton, and John Schwartz for their support and assistance for these efforts. Igor Nesterenko provided valuable help and guidance with digital cameras and optics for plasma imaging and monitoring. This work was a collaborative effort with the FRIB cryogenics team, the FRIB cavity preparation team, and the rest of the FRIB laboratory.

We thank the plasma teams at SNS, Jefferson Lab, Fermilab, IJCLab, and Argonne for useful discussions, information sharing, and suggestions. We are especially thankful to colleagues at SNS and Fermilab who shared their plasma processing expertise. The encouragement from Fermilab colleagues to implement network analyzer monitoring of the resonant frequency was particularly valuable.

ISBN: 978-3-95450-234-9 ISSN: 2673-5504 doi:10.18429/JACoW-SRF2023-THIXA01

REFERENCES

[1] S.-H. Kim *et al.*, "Overview of ten-year operation of the superconducting linear accelerator at the Spallation Neutron Source," *Nucl. Instrum. Methods. Phys. Res. A*, vol. 852, pp. 20–32, Apr. 2017. doi:10.1016/j.nima.2017.02.009

[2] B. Giaccone *et al.*, "Plasma Processing to Reduce Field Emission in LCLS-II 1.3 GHz SRF Cavities," in *Proc. 19th Int. Conf. RF Superconductivity (SRF'19)*, Dresden, Germany, Jun.-Jul. 2019, pp. 1231–1238. doi:10.18429/JACoW-SRF2019-FRCAB7

[3] A. Wu *et al.*, "In-situ plasma cleaning to decrease the field emission effect of half-wave superconducting radio-frequency cavities," *Nucl. Instrum. Methods. Phys. Res. A*, vol. 905, pp. 61–70, Oct. 2018. doi:10.1016/j.nima.2018.07.039

[4] S. C. Huang, Q. W. Chu, Y. He, C. L. Li, A. D. Wu, and S. X. Zhang, "The Effect of Helium Processing and Plasma Cleaning for Low Beta HWR Cavity," in *Proc. 19th Int. Conf. RF Superconductivity (SRF'19)*, Dresden, Germany, Jun.-Jul. 2019, pp. 1228–1230. doi:10.18429/JACoW-SRF2019-FRCAB6

[5] P. Berrutti, "Plasma cleaning R&D at FNAL," presented at the June 2018 TeSLA Technology Collaboration Meeting, Saitama, Japan.

[6] B. Giaccone *et al.*, "Plasma cleaning of the SLAC Linac Coherent Light Source II high energy verification cryomodule cavities," *Phys. Rev. Accel. Beams*, vol. 25, p. 102 001, Oct. 2022. doi:10.1103/PhysRevAccelBeams.25.102001

[7] T. Powers, N. C. Brock, and T. D. Ganey, "In Situ Plasma Processing of Superconducting Cavities at Jefferson Lab," in *Proc. 20th Int. Conf. RF Superconductivity (SRF'21)*, East Lansing, MI, USA, Oct. 2022, pp. 485–489. doi:10.18429/JACoW-SRF2021-TUPTEV004

[8] T. Powers, N. C. Brock, and T. D. Ganey, "In Situ Plasma Processing of Superconducting Cavities at JLab," in *Proc. North American Particle Accelerator Conf. (NAPAC'22)*, Albuquerque, NM, USA, Nov. 2022, pp. 22–25. doi:10.18429/JACoW-NAPAC2022-MOYE5

[9] J. Wei *et al.*, "Accelerator commissioning and rare isotope identification at the Facility for Rare Isotope Beams," *Mod. Phys. Lett. A*, vol. 37, no. 09, p. 2 230 006, Mar. 2022. doi:10.1142/S0217732322300063

[10] J. Wei *et al.*, "FRIB Transition to User Operations, Power Ramp Up, and Upgrade Perspectives," presented at SRF'23, Grand Rapids, MI, USA, Jun. 2023, paper MOIAA01, this conference.

[11] C. Zhang *et al.*, "Development of In-Situ Plasma Cleaning for the FRIB SRF Linac," in *Proc. 20th Int. Conf. RF Superconductivity (SRF'21)*, Virtual Conference, Oct. 2022, pp. 657–661. doi:10.18429/JACoW-SRF2021-WEPTEV011

[12] W. Hartung *et al.*, "Plasma Processing of Superconducting Quarter-Wave Resonators Using a Higher-Order Mode," in *Proc. North American Particle Accelerator Conf. (NAPAC'22)*, Albuquerque, NM, USA, Nov. 2022, pp. 267–270. doi:10.18429/JACoW-NAPAC2022-MOPA91

[13] A. D. Wu *et al.*, "The Destructive Effects to the RF Coupler by the Plasma Discharge," in *Proc. 19th Int. Conf. RF Superconductivity (SRF'19)*, Dresden, Germany, Jun.-Jul. 2019, pp. 285–287. doi:10.18429/JACoW-SRF2019-MOP085

[14] P. R. Tutt, W. Hartung, S. H. Kim, and T. Xu, "Investigation of Coupler Breakdown Thresholds for Plasma Processing of FRIB Quarter-Wave Resonators with Fundamental and Higher-Order Modes," presented at SRF'23, Grand Rapids, MI, USA, Jun. 2023, paper WEPWB127, this conference.

[15] M. A. Lieberman and A. J. Lichtenberg, *Principles of Plasma Discharges and Materials Processing*, Second Edition. Wiley, 2005, Section 4.6.

[16] M. Doleans *et al.*, "Plasma Processing R&D for the SNS Superconducting Linac RF Cavities," in *Proc. 16th Int. Conf. RF Superconductivity (SRF'13)*, Paris, France, Sep. 2013, pp. 551–557. https://jacow.org/SRF2013/papers/TUP057.pdf

[17] P. Berrutti *et al.*, "Plasma ignition and detection for in-situ cleaning of 1.3 GHz 9-cell cavities," *J. Appl. Phys.*, vol. 126, p. 023 302, Jul. 2019. doi:10.1063/1.5092235

[18] M. Doleans, "Plasma Processing Boosts the Energy of the Spallation Neutron Source Superconducting Linac," FRIB Accelerator Physics and Engineering Virtual Seminar, 22 October 2021.

[19] M. Doleans, "Ignition and monitoring technique for plasma processing of multicell superconducting radio-frequency cavities," *J. Appl. Phys.*, vol. 120, p. 243 301, Dec. 2016. doi:10.1063/1.4972838